Centrifugal Micro-Channel Array Droplet Generation for Highly Parallel Digital PCR

Article *in* Lab on a Chip · December 2016

DOI: 10.1039/C6LC01305H

6 authors, including:

Peiyu Liao
Peking University
8 PUBLICATIONS **97** CITATIONS

SEE PROFILE

Yanyi Huang
Peking University
232 PUBLICATIONS **7,821** CITATIONS

SEE PROFILE

Volume 17 | Number 2 | 21 January 2017 | Pages 201–352

Lab on a Chip

Miniaturisation for chemistry, physics, biology, materials science and bioengineering

rsc.li/loc

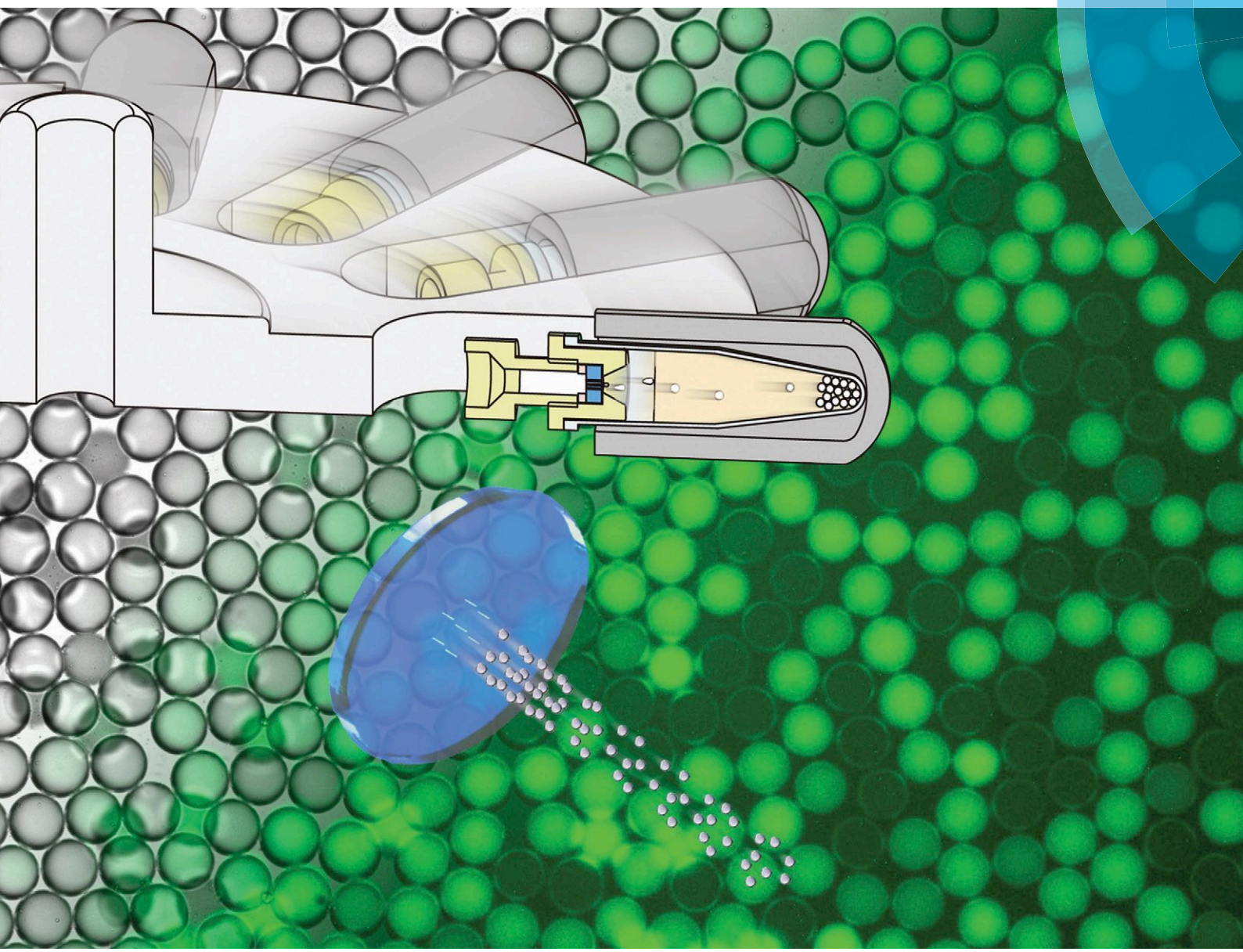

ISSN 1473-0197

ROYAL SOCIETY OF CHEMISTRY

COMMUNICATION

Yanyi Huang *et al.*

Centrifugal micro-channel array droplet generation for highly parallel digital PCR

Lab on a Chip

COMMUNICATION

Centrifugal micro-channel array droplet generation for highly parallel digital PCR†

Zitian Chen,[a] Peiyu Liao,[a] Fangli Zhang,[a] Mengcheng Jiang,[a] Yusen Zhu[b] and Yanyi Huang*[a]

Cite this: *Lab Chip*, 2017, **17**, 235

Received 20th October 2016,
Accepted 6th December 2016

DOI: 10.1039/c6lc01305h

www.rsc.org/loc

Stable water-in-oil emulsion is essential to digital PCR and many other bioanalytical reactions that employ droplets as microreactors. We developed a novel technology to produce monodisperse emulsion droplets with high efficiency and high throughput using a bench-top centrifuge. Upon centrifugal spinning, the continuous aqueous phase is dispersed into monodisperse droplet jets in air through a micro-channel array (MiCA) and then submerged into oil as a stable emulsion. We performed dPCR reactions with a high dynamic range through the MiCA approach, and demonstrated that this cost-effective method not only eliminates the usage of complex microfluidic devices and control systems, but also greatly suppresses the loss of materials and cross-contamination. MiCA-enabled highly parallel emulsion generation combines both easiness and robustness of picoliter droplet production, and breaks the technical challenges by using conventional lab equipment and supplies.

Quantitative measurement of DNA or RNA is extremely critical in modern biology and medical applications. Real-time quantitative polymerase chain reaction (qPCR) has become an essential tool for detecting trace amounts of DNA or RNA (through reverse transcription PCR, RT-PCR) with specific sequences, providing the most sensitive method to quantify the copy number of target sequences.[1–6] However, absolute quantification is still a challenge for most qPCR assays. Digital PCR (dPCR), an end-point assay that distributes target DNAs into a large number of partitions and counts those positively reacted partitions, has become more and more promising in quantifying the absolute number of rare targets.[7–14] The target distribution among the partitions follows the Poisson statistics, which also helps to convert digital counts into analog concentrations if needed.[12,15–17] Recently, dPCR has shown auspicious trends in many medical applications, such as the detection of pathogenic genes,[18–21] minority alleles,[7,11,22] or copy number variations,[23,24] and the highly accurate quantification of gene expression.[25]

Partition can be experimentally realized by dividing the PCR reaction solution into hundreds or thousands of microcentrifuge tubes/vials,[7] nanoliter to femtoliter reaction chambers in polymer- or glass-made microfluidic devices,[12,16,25–28] or water-in-oil (w/o) emulsion droplets.[8,10,11,29,30] Currently, emulsion-based approaches have become the most popular method used in research and medical laboratories.[31] They exhibit a few intrinsic advantages. First, an optimized microfluidic emulsion generator, which employs water-immiscible oil to effectively pinch the aqueous flow into monodisperse droplets, can produce a large amount of droplets with the size of picoliters to nanoliters within a short period of time. Second, the phase separation between oil and water phases naturally segregates droplets without extra operation. Third, all the isolated reactions can be pulled together and then become a single reaction using a conventional PCR machine. However, the cost of microfluidic chip-based emulsion-generating devices, as well as their control instruments, is still relatively high. Not only are in-house designed microfluidic devices too complex to be adapted by other labs, but also many commercially available instruments require extra skills to process properly.

In droplet dPCR, uniform partition is a crucial prerequisite for high accuracy due to the premise of the Poisson distribution of target DNA fragments. Besides, the number of partitions directly influences the resolution, accuracy and dynamic range of a dPCR assay. An ideal dPCR assay should be easy and fast to operate in most laboratories, with minimum liquid transfer steps to avoid material loss or cross-contamination, and a dynamic range (partition number) of up to hundreds of thousands. In a typical dPCR workflow, there are three major steps: droplet generation and emulsification, thermal cycling for PCR amplification, and positive/negative compartment counting. In this work, we focus on addressing

[a] *Biodynamic Optical Imaging Center (BIOPIC), Beijing Advanced Innovation Center for Genomics (ICG), Peking-Tsinghua Center for Life Sciences, and College of Engineering, Peking University, Beijing, China. E-mail: yanyi@pku.edu.cn*
[b] *Integrated Science Program, Yuanpei College, Peking University, Beijing, China*
† Electronic supplementary information (ESI) available: Supporting figures and text. See DOI: 10.1039/c6lc01305h

two major technical challenges related to the first two steps. We developed an off-chip monodisperse droplet generation method that can efficiently produce w/o emulsion using a bench-top centrifuge machine, one of the most popular instruments in the lab.

With a cost-effective and highly precise micro-channel array (MiCA), the aqueous solution can be dispersed into stable picoliter-droplets and then PCR thermal cycling without extra liquid transfer in microcentrifuge tubes can be performed, significantly reducing the difficulty and complexity of performing droplet-based biological and chemical assays, and minimizing the loss of rare input materials by eliminating the dead volume. Unlike microfluidic approaches, which involve exquisite control on pressure or flow rates and delicate micro-fabrication processes, by virtue of centrifugation, this novel emulsion generation method is intrinsically highly parallel given that many samples can be processed simultaneously without contamination.

The general process of MiCA-emulsification is shown in Fig. 1. As the most critical component to ensure monodisperse water-in-oil (w/o) emulsion, each hydrophobic MiCA plate contains a number of through-holes with identical size. A polyetheretherketone (PEEK) container with a MiCA is assembled and inserted into a conventional microcentrifuge tube placed in the swing bucket rotor of a centrifuge. The aqueous solution (PCR mixture) is placed on the top of the MiCA. Since the size of the microchannel is small, the solution will not flow through the MiCA but be held by surface tension. When the rotor spins, the greatly elevated centrifugal force will drive the solution to flow through the MiCA at high speed. The aqueous solution ejected out of the MiCA will be continuously pinched off at the nozzles and then completely transformed into small droplets that fly into the receiving oil to form w/o emulsion. By tuning the spinning speed and changing the MiCA with different channel numbers or sizes, we are able to generate droplets of various sizes.

The fabrication of the MiCA (Fig. 2) was inspired by the process used in micro-channel plate manufacturing in the photomultiplier tube industry.[32] Two types of glass fibers were carefully aligned and tightly arranged to form a bundle with hexagonal lattice symmetry. A few acid-soluble fibers, made of glass with high doping ratios of rare earth (RE) oxides, were placed inside the bundle. This bundle was melted and stretched into a glass rod with a diameter of a few mm using a pulling tower. Thus, each fiber in the bundle was pulled in geometrical proportion into a few μm in diameter. The rod was then sliced into thin plates, and the fiber-array plates were later polished to optical flatness for both facets.

Having been etched by nitric acid (0.3 mol L^{-1}) for 20 h and subjected to ultrasonication, those RE-doped fibers in the polished slices were dissolved, leaving through-channels in the fiber-array. These array plates were treated with oxygen plasma for surface activation and then fumigated with 1*H*,1*H*,2*H*,2*H*-perfluoro-octyltrichlorosilane (PFOTCS) vapor to form a hydrophobic monolayer. Each MiCA is a disk, 4.5 mm in diameter and 1.0 mm thick, with seven equidistantly spaced 6.2 μm micro-channels.

We designed a container to hold the MiCA. A pair of threaded nut and fitting are made of PEEK, between which a PTFE gasket and a MiCA were sandwiched (Fig. 1a and b). The nut has an outpointing flange to support itself on the edge of a microcentrifuge tube. The assembly is preferred to

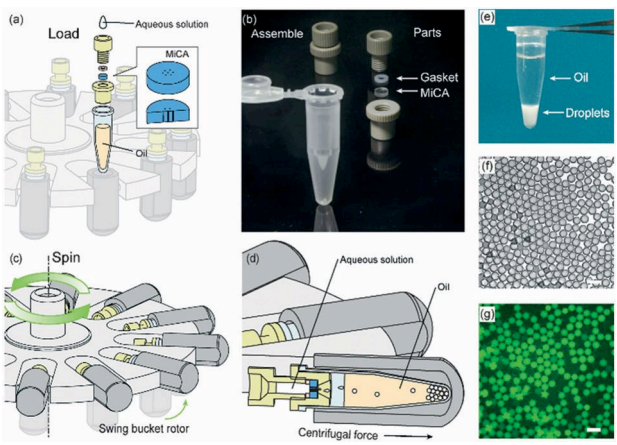

Fig. 1 Construction and operation principle of the MiCA-emulsifier. (a) Assembly of a container with the MiCA. The main body was made of PEEK with a PTFE gasket ring. (b) The components. (c) The swing buckets with microcentrifuge tubes and MiCA inserts will flip centripetally when spinning. (d) During spinning, the centrifugal force is perpendicular to the MiCA plate, breaking the solution into small droplets which then form emulsion in the receiving oil. (e) The emulsion stably sits at the bottom of a microcentrifuge tube after centrifugation. (f) Microphotograph of emulsion droplets after 40 thermal cycles of PCR. (g) Fluorescence microphotograph indicating the digital amplification within the emulsion. Scale bars: 100 μm.

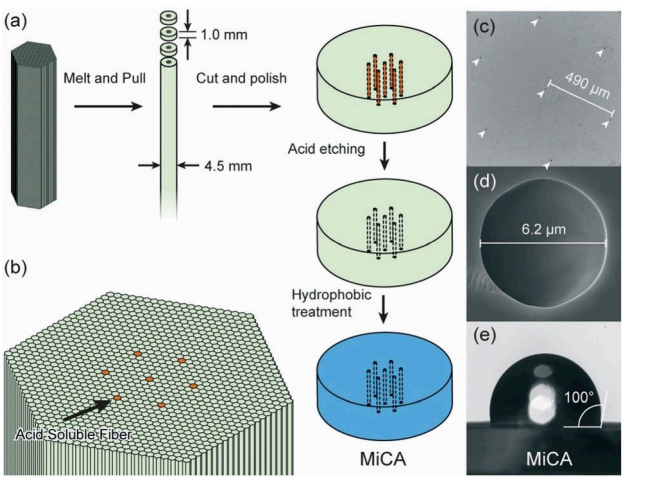

Fig. 2 The fabrication procedure and characteristics of the MiCA. (a) A glass fiber bundle is pulled into a rod, and then sliced into thin disks. (b) Within the bundles, there are a few acid-soluble fibers with high doping ratios of rare earth element oxides. Sliced fiber arrays are fine polished and etched in nitric acid to form through-holes. The surface of the MiCA was activated by oxygen plasma and then treated with fluorinated silane vapor. (c) SEM micrograph of the MiCA facet with 7 micro-channels (indicated as arrows). (d) SEM picture of a channel opening. (e) Contact angle of water on the MiCA surface.

be operated in a dust-free environment and the aqueous solution needs to be filtered prior to experiment to prevent clogging of the micro-channels (Fig. 2c and d).

The formulation of the two immiscible phases is critical to the characteristics and stability of w/o emulsion. First, the density of the oil has to be lower than that of water, thus the received flying droplets will sink into the bottom of the tube during centrifugation. However, the density difference between oil and water needs to be small, providing enough buoyancy to ensure that the droplets do not merge together. Second, low viscosity (*ca.* 10 cSt) of the oil is preferred, ensuring that the aqueous droplets can easily enter the oil–air interface without being smashed. Third, the formula of the oil and surfactant should be PCR-compatible. Although other microfluidic emulsion generators have optimized a few formulas, they do not perform well enough in our approach. Mineral oil formulas[33,34] have been widely used in flow-focusing emulsion generators, however, such highly viscous oil phases will cause droplets to be smashed in our case and hence cannot be used. We developed a new oil formula, a binary mixture of 93% (v/v) isopropyl palmitate (Sigma-Aldrich) and 7% (v/v) ABIL EM180 (Evonik), with a density of 0.85 g cm^{-3} and a viscosity of 12 cSt, which has been proven to be fully compatible with the PCR buffer used in our experiment. This new formula has exhibited remarkable stabilizing and compartmentalizing capability for monodisperse droplet emulsion as well as heat resistance, a prerequisite for droplet digital PCR.

The size and uniformity of droplets are determined by two major factors, the size of the micro-channels and the centrifugal force. In general, smaller holes and higher centrifugal force will favor smaller droplets in emulsion. We found that the optimal size of the holes was about 6 μm for generating high-quality w/o emulsion. We assessed how the centrifugal force affected droplet uniformity (Fig. 3). Low spinning speed will inevitably produce small droplets and hence severely reduces the uniformity of droplets. One of the possible reasons for the formation of small droplets is that, under low centrifugal force, the liquid flow velocity within the micro-channels is not great enough and causes the pinched tail of a main droplet to break into smaller droplets. The droplets become monodisperse, and smaller in average, with the elevation of centrifugal speed. The transition between the polydisperse droplet and monodisperse droplet regimes falls around 5000*g*.

We performed a digital PCR (dPCR) test using MiCA-generated emulsion droplets, and compared the result with that of a commercial machine with a microfluidic chip-based droplet generator (QX200, Bio-Rad). The template was a 280 bp double-stranded DNA fragment, whose sequence was from the prfA gene in *L. monocytogenes*. The total aqueous volume of each dPCR is 20 μl, with 10 μl of sample and 10 μl of premix buffer containing polymerase, primers, and TaqMan probes. With the centrifugal force at 13 000*g*, the 20 μl reaction mix will completely transform into liquid droplets with zero dead volume. The whole process takes less than 7 min,

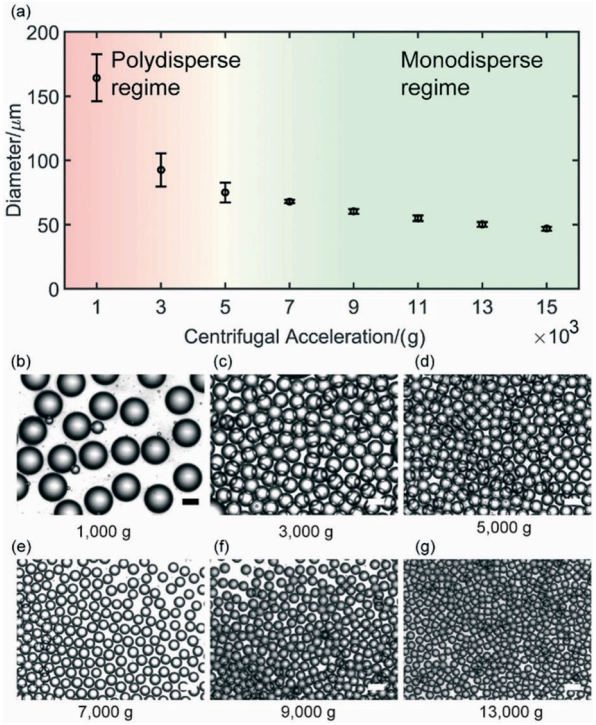

Fig. 3 The size and morphology of droplets generated under varied centrifugal speed. (a) The size of droplets generated at different centrifugal speeds, with error bars representing the standard deviation of droplet diameter. Droplet sizes with standard deviation (μm) and numbers of droplets examined (*n*): 164.3 ± 18.3 (*n* = 93), 92.4 ± 12.9 (*n* = 621), 74.8 ± 7.8 (*n* = 1013), 67.9 ± 1.3 (*n* = 179), 60.1 ± 1.9 (*n* = 196), 54.9 ± 2.2 (*n* = 247), 50.2 ± 1.8 (*n* = 333), 46.8 ± 1.6 (*n* = 269). (b–g) Microscopy images of the droplets generated under varied centrifugal force. Scale bars: 100 μm.

resulting in highly uniform droplets with a diameter of 52.5 μm.

The PCR thermocycling was performed directly with the receptor microcentrifuge tubes on conventional PCR machines. After PCR, the droplets were divided into two groups – fluorescent 'positive' ones indicating the existence of the template DNA and the non-fluorescent 'negative' ones (Fig. 1g). Droplet counting was performed using a modified flow cytometer to measure the fluorescence signals of each droplet in the emulsion. We pressurized the emulsion through a flow cell made of a glass micro-pipette with a narrow neck, whose inner-diameter was about 100 μm. The fluorescence signal of each droplet was captured through a green fluorescent channel (530 ± 20 nm) excited by a 488 nm laser. A DAQ card was used to record the raw signal of photomultiplier tubes for further analysis. This system provides distinct discrepancy between the positive and negative signals, causing a negligible identification error.

We carried out dPCR tests for 10 samples, three replicates each, with different concentrations of target template DNA from a few copies per μl to ~2000 copies per μl (Fig. 4). The two experimental approaches are highly concordant (Fig. 4b). We found that although serial flow detection schemes, such as our modified flow cytometer or QX200 instruments,

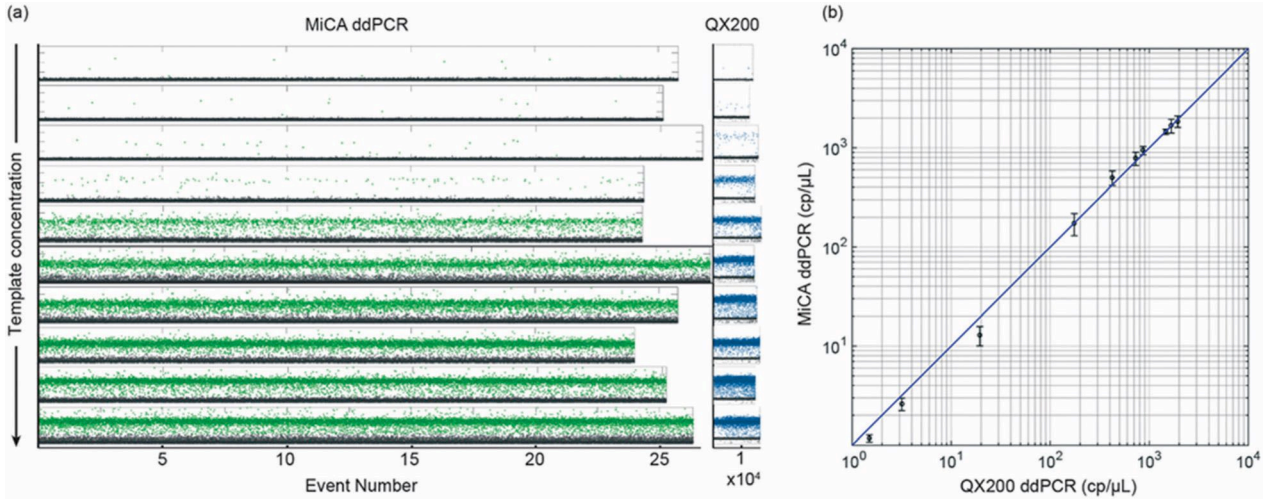

Fig. 4 The results of digital PCR performed using the MiCA emulsion generator, compared to the results using the Bio-Rad ddPCR QX200 platform. (a) Each dot stands for an effective droplet readout. If its fluorescence is above a threshold, a droplet is identified as positive (green for MiCA, blue for QX200), otherwise it is negative (grey). (b) The concordance between the results from the two approaches. Error bars are the standard deviations.

exhibit the sensitivity necessary to capture every single droplet, in fact neither approach can capture all the droplets because of the incomplete emulsion transfer and the instability time-window at the beginning and the end of the counting process. Ideally, for each 20 μl sample, we should detect about 2.4×10^4 droplets, with a droplet volume of 0.85 nl using QX200,[35,36] or about 3.0×10^5 droplets, with a diameter around 50 μm using the MiCA emulsion generator. Thus, the drop-out rates of detection are 37% $[100\% - (1.5 \times 10^4/2.4 \times 10^4) \times 100\%]$ for QX200 and 17% $[100\% - (2.5 \times 10^5/3.0 \times 10^5) \times 100\%]$ for the MiCA. This significantly reduced drop-out rate will benefit the applications that require absolute counting of positive droplets with much higher accuracy. Compared to the Bio-Rad ddPCR system, our approach provides a much higher dynamic range due to the smaller size of the droplets. Such a high dynamic range is desired in many applications especially when the target DNA or RNA copies vary in a big range, or when the expression level of many genes follows bimodal distribution in single-cell studies. In addition, a higher dynamic range also benefits the accuracy of absolute counting due to the Poisson statistics. When the concentration of the DNA template is 150 copies per μl, in QX200-generated emulsion there would be 11.75% droplets that are positive and 0.74% of the total droplets have more than one copy, while in MiCA-generated emulsion there would be 1.00% positive droplets with less than 0.005% droplets containing more than one copy. By virtue of mass droplets of the MiCA tube, it is possible to achieve single molecule compartmentalization with unprecedented easiness.

In summary, we have developed a new technology that utilizes centrifugal force to produce a large amount ($>10^5$) of picoliter-size monodisperse w/o emulsion droplets within a few minutes. Although the centrifugal capillary for gel particle generation has been reported,[37] our invention stands out because its multiple channels can greatly elevate the droplet generation efficiency. In addition, this parallel-channel design is tolerant of blockage.

MiCA can be massively manufactured by extant industrial facilities with high reproducibility, thus significantly simplifying the generation process of high-quality emulsion, which has been conventionally produced using microfluidic chips. Furthermore, this work has solved the thermocycling-resistant emulsification problem that precludes numerous droplet generation devices from performing digital PCR. With the optimized oil recipe, such emulsion exhibits excellent mechanical and thermal stabilities. This method is built on a bench-top centrifuge, one of the mostly available instruments in any biology and chemistry labs, and seamlessly offers emulsion generation in a highly parallel manner with great scalability. The fabrication of the MiCA plates can be cost-effective compared to that of PDMS- and glass-based microfluidic chips due to the massive production capacity of the micro-channel plate technique. We have tested the dPCR performance using MiCA-generated emulsion. Our new method not only provides a larger dynamic range but also a better recovery rate of droplets during detection.

The simplicity and handiness of this new technique have made dPCR cost-effective and plausible to be adapted by many labs. The emulsion recipe, which can stabilize the droplets through jetting from air to oil and resist thermal cycling, should also be valuable to many other analytical and biochemical applications that utilize droplets as versatile and malleable microreactors.[13,14,18,27,38–48] This method, however, is still facing a bottleneck – the detection scheme of serial detection is still far from being ideal or elegant. Furthermore, exposure of the amplified DNA product to the experimental environment is very likely to interfere in quantitative DNA assays afterwards and such contamination needs to be completely eliminated for medical research and diagnosis. Transferring the emulsion droplets from the PCR

microcentrifuge tubes into counting equipment may introduce unwanted contamination. Hence, we envision that, to make the MiCA approach more accessible, much effort needs to be focused on the development of simple but accurate detection methodologies to couple with the emulsion generator.

Acknowledgements

The authors thank Shuo Qiao, Li Kang and Xuanyang Chen for experimental assistance, and Wenxiong Zhou and Dr. Haifeng Duan for fruitful discussion. This work was supported by the Ministry of Science and Technology of China (2015AA0200601 and 2016YFC0900100) and the National Natural Science Foundation of China (21327808 and 21525521).

References

1 P. M. Holland, R. D. Abramson, R. Watson and D. H. Gelfand, *Proc. Natl. Acad. Sci. U. S. A.*, 1991, **88**, 7276–7280.
2 C. A. Heid, J. Stevens, K. J. Livak and P. M. Williams, *Genome Res.*, 1996, **6**, 986–994.
3 K. J. Livak and T. D. Schmittgen, *Methods*, 2001, **25**, 402–408.
4 M. W. Pfaffl, *Nucleic Acids Res.*, 2001, **29**, e45.
5 T. Nolan, R. E. Hands and S. A. Bustin, *Nat. Protoc.*, 2006, **1**, 1559–1582.
6 B. A. Z. Thomas and D. Schmittgen, *J. Biochem. Biophys. Methods*, 2000, **46**, 69–81.
7 B. Vogelstein and K. W. Kinzler, *Proc. Natl. Acad. Sci. U. S. A.*, 1999, **96**, 9236–9241.
8 A. C. Hatch, J. S. Fisher, A. R. Tovar, A. T. Hsieh, R. Lin, S. L. Pentoney, D. L. Yang and A. P. Lee, *Lab Chip*, 2011, **11**, 3838.
9 A. C. Hatch, J. S. Fisher, S. L. Pentoney, D. L. Yang and A. P. Lee, *Lab Chip*, 2011, **11**, 2509–2517.
10 B. J. Hindson, K. D. Ness, D. A. Masquelier, P. Belgrader, N. J. Heredia, A. J. Makarewicz, I. J. Bright, M. Y. Lucero, A. L. Hiddessen, T. C. Legler, T. K. Kitano, M. R. Hodel, J. F. Petersen, P. W. Wyatt, E. R. Steenblock, P. H. Shah, L. J. Bousse, C. B. Troup, J. C. Mellen, D. K. Wittmann, N. G. Erndt, T. H. Cauley, R. T. Koehler, A. P. So, S. Dube, K. A. Rose, L. Montesclaros, S. Wang, D. P. Stumbo, S. P. Hodges, S. Romine, F. P. Milanovich, H. E. White, J. F. Regan, G. A. Karlin-Neumann, C. M. Hindson, S. Saxonov and B. W. Colston, *Anal. Chem.*, 2011, **83**, 8604–8610.
11 D. Pekin, Y. Skhiri, J.-C. Baret, D. L. Corre, L. Mazutis, C. B. Salem, F. Millot, A. E. Harrak, J. B. Hutchison, J. W. Larson, D. R. Link, P. Laurent-Puig, A. D. Griffiths and V. Taly, *Lab Chip*, 2011, **11**, 2156.
12 F. Shen, B. Sun, J. E. Kreutz, E. K. Davydova, W. Du, P. L. Reddy, L. J. Joseph and R. F. Ismagilov, *J. Am. Chem. Soc.*, 2011, **133**, 17705–17712.
13 A. S. Whale, J. F. Huggett, S. Cowen, V. Speirs, J. Shaw, S. Ellison, C. A. Foy and D. J. Scott, *Nucleic Acids Res.*, 2012, **40**, e82.
14 C. M. Hindson, J. R. Chevillet, H. A. Briggs, E. N. Gallichotte, I. K. Ruf, B. J. Hindson, R. L. Vessella and M. Tewari, *Nat. Methods*, 2013, **10**, 1003–1005.
15 L. A. Warren, J. A. Weinstein and S. R. Quake, *The Digital Array Response Curve*, 2007, pp. 1–9, https://quakelab.stanford.edu/quake-lab-publications.
16 S. Dube, J. Qin and R. Ramakrishnan, *PLoS One*, 2008, **3**, e2876.
17 N. Majumdar, T. Wessel and J. Marks, *PLoS One*, 2015, **10**, e0118833.
18 R. A. White, 3rd, S. R. Quake and K. Curr, *J. Virol. Methods*, 2012, **179**, 45–50.
19 M. C. Strain, S. M. Lada, T. Luong, S. E. Rought, S. Gianella, V. H. Terry, C. A. Spina, C. H. Woelk and D. D. Richman, *PLoS One*, 2013, **8**, e55943.
20 R. H. Sedlak and K. R. Jerome, *Diagn. Microbiol. Infect. Dis.*, 2013, **75**, 1–4.
21 A. S. Devonshire, I. Honeyborne, A. Gutteridge, A. S. Whale, G. Nixon, P. Wilson, G. Jones, T. D. McHugh, C. A. Foy and J. F. Huggett, *Anal. Chem.*, 2015, **87**, 3706–3713.
22 N. B. Tsui, R. A. Kadir, K. C. Chan, C. Chi, G. Mellars, E. G. Tuddenham, T. Y. Leung, T. K. Lau, R. W. Chiu and Y. M. Lo, *Blood*, 2011, **117**, 3684–3691.
23 Y. M. Lo, F. M. Lun, K. C. Chan, N. B. Tsui, K. C. Chong, T. K. Lau, T. Y. Leung, B. C. Zee, C. R. Cantor and R. W. Chiu, *Proc. Natl. Acad. Sci. U. S. A.*, 2007, **104**, 13116–13121.
24 H. C. Fan and S. R. Quake, *Anal. Chem.*, 2007, **79**, 7576–7579.
25 L. Warren, D. Bryder, I. L. Weissman and S. R. Quake, *Proc. Natl. Acad. Sci. U. S. A.*, 2006, **103**, 17807–17812.
26 K. A. Heyries, C. Tropini, M. Vaninsberghe, C. Doolin, O. I. Petriv, A. Singhal, K. Leung, C. B. Hughesman and C. L. Hansen, *Nat. Methods*, 2011, **8**, 649–651.
27 R. Sanders, J. F. Huggett, C. A. Bushell, S. Cowen, D. J. Scott and C. A. Foy, *Anal. Chem.*, 2011, **83**, 6474–6484.
28 Y. Men, Y. Fu, Z. Chen, P. A. Sims, W. J. Greenleaf and Y. Huang, *Anal. Chem.*, 2012, **84**, 4262–4266.
29 Q. Zhong, S. Bhattacharya, S. Kotsopoulos, J. Olson, V. Taly, A. D. Griffiths, D. R. Link and J. W. Larson, *Lab Chip*, 2011, **11**, 2167.
30 H. Yamashita, M. Morita, H. Sugiura, K. Fujiwara, H. Onoe and M. Takinoue, *J. Biosci. Bioeng.*, 2015, **119**, 492–495.
31 M. Baker, *Nat. Methods*, 2012, **9**, 541–544.
32 S. Dhawan, *IEEE Trans. Nucl. Sci.*, 1981, **NS-28**, 672–676.
33 J. C. Baret, *Lab Chip*, 2012, **12**, 422–433.
34 K. R. Pandit, P. E. Rueger, R. V. Calabrese, S. R. Raghavan and I. M. White, *Colloids Surf., B*, 2015, **126**, 489–495.
35 P. Corbisier, L. Pinheiro, S. Mazoua, A. M. Kortekaas, P. Y. Chung, T. Gerganova, G. Roebben, H. Emons and K. Emslie, *Anal. Bioanal. Chem.*, 2015, **407**, 1831–1840.
36 L. Dong, Y. Meng, Z. Sui, J. Wang, L. Wu and B. Fu, *Sci. Rep.*, 2015, **5**, 13174.
37 K. Maeda, H. Onoe, M. Takinoue and S. Takeuchi, *Adv. Mater.*, 2012, **24**, 1340–1346.
38 D. T. Chiu, R. M. Lorenz and G. D. M. Jeffries, *Anal. Chem.*, 2009, **81**, 5111–5118.
39 R. A. White, 3rd, P. C. Blainey, H. C. Fan and S. R. Quake, *BMC Genomics*, 2009, **10**, 116.

40 A. B. Theberge, F. Courtois, Y. Schaerli, M. Fischlechner, C. Abell, F. Hollfelder and W. T. Huck, *Angew. Chem., Int. Ed.*, 2010, **49**, 5846–5868.
41 P. C. Blainey and S. R. Quake, *Nucleic Acids Res.*, 2011, **39**, e19.
42 A. Gansen, A. M. Herrick, I. K. Dimov, L. P. Lee and D. T. Chiu, *Lab Chip*, 2012, **12**, 2247–2254.
43 H. N. Joensson and H. Andersson Svahn, *Angew. Chem., Int. Ed.*, 2012, **51**, 12176–12192.
44 T. D. Rane, L. Chen, H. C. Zec and T. H. Wang, *Lab Chip*, 2015, **15**, 776–782.
45 Y. Fu, C. Li, S. Lu, W. Zhou, F. Tang, X. S. Xie and Y. Huang, *Proc. Natl. Acad. Sci. U. S. A.*, 2015, **112**, 11923–11928.
46 H. S. Han, P. G. Cantalupo, A. Rotem, S. K. Cockrell, M. Carbonnaux, J. M. Pipas and D. A. Weitz, *Angew. Chem., Int. Ed.*, 2015, **54**, 13985–13988.
47 A. K. Price and B. M. Paegel, *Anal. Chem.*, 2016, **88**, 339–353.
48 D. van Swaay, T. Y. Tang, S. Mann and A. de Mello, *Angew. Chem., Int. Ed.*, 2015, **54**, 8398–8401.

Electronic Supplementary Material (ESI) for Lab on a Chip.

Supplementary Information

Centrifugal Micro-Channel Array Droplet Generation for Highly Parallel Digital PCR

Zitian Chen,[a] Peiyu Liao,[a] Fangli Zhang,[a] Mengcheng Jiang,[a] Yusen Zhu,[b] and Yanyi Huang*[a]

[a] *Biodynamic Optical Imaging Center (BIOPIC), Beijing Advanced Innovation Center for Genomics (ICG), Peking-Tsinghua Center for Life Sciences, and College of Engineering, Peking University, Beijing, China*

[b] *Integrated Science Program, Yuanpei College, Peking University, Beijing, China*

*Corresponding author. E-mail: yanyi@pku.edu.cn

1. Centrifugation process

The process of centrifugation includes three stages in terms of rotating speed: speeding-up, steady spinning, and braking. As is demonstrated in **Figure 3**, the size of droplet closely linked to the rotating speed. Thus in order for a uniform and monodisperse micro-emulsion, one should avoid droplet generation in speeding-up and braking stages so that most of droplets are generated under steady rotating speed. Extending set centrifuge duration is a feasible method for droplet generation such that the aqueous liquid would be exhausted before entering the braking stage (**Figure S1**). The accelerating stage is nonetheless inevitable. To yield emulsion droplets with better monodispersity we investigated the number of the microchannels in a single MiCA plate. By reducing the number of the channels, the overall flow rate is reduced so that the proportion of the fluid flowing during accelerating stage decreases. When the set acceleration is above 10,000 g, our centrifuge machine only takes 10 seconds to reach full speed, leaving more than ~98% sample becoming droplet during steady spinning stage.

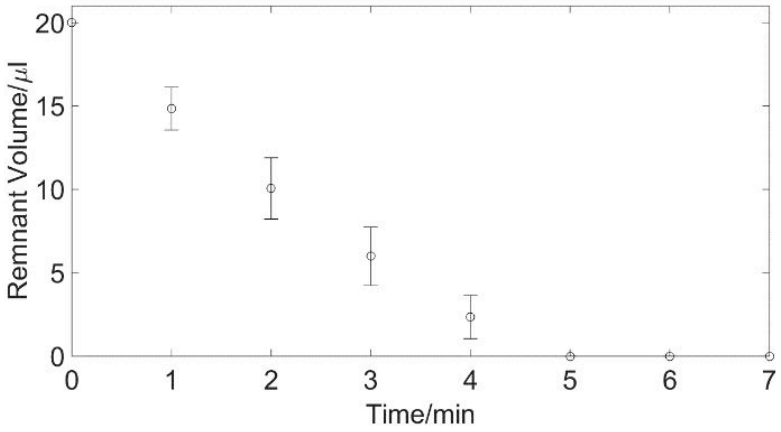

Figure S1. Remnant volume of 20 μl sample, spun at 130,000 $m \cdot s^{-2}$ for different time.

2. MiCA plate surface treatment

The surface hydrophobicity treatment of the glass slices included acid washing with Piranha solution (*CAUTION: Piranha solution is extremely energetic and may result in explosion or skin burns if not handled with extreme caution!*) oxygen plasma activation, perfluoroalkyl silane vapor deposition and isopropyl ethanol washing. We submerged the MiCA plates in Piranha solution prepared beforehand and subjected them to ultrasonication for 10 min. Having been washed with DI water and dried under 70 ℃ for 20 min, the MiCA slices were put into an oxygen plasma cleaner (Chengdu Mingheng PDC-MG) for surface activation (5.5 min, 890 V, 220 mA, 7.0 Pa). Then we transferred the activated glass slices into a vacuum desiccator, which contains an open vial with 200 μl 1H,1H,2H,2H-perfluorooctyltrichlorosilane (PFOTCS) (Sigma). We later vacuumed the desiccator to less than 0.1 psi for 50 min. Subsequently, we heated the MiCA on a hotplate for 5 min at 120 ℃. We finally washed the MiCA plates with isopropyl ethanol (MOS grade) and then again with DI water, dried them in ambient environment.

3. Digital PCR assays

The oligonucleotide sequences are listed in **Table S1**. The target DNA was first chemically synthesized and confirmed by Sanger sequencing and then PCR amplified. The prfA sequence was first PCR amplified with forward and reverse amplification primers (Q5® High-Fidelity 2X Master Mix, 95℃ 2 min activation, 32 cycles of 94℃ denaturing 15 seconds, and 60℃ annealing and extension 30 seconds) and then purified with agarose-gel electrophoresis. Recovered DNA concentration was roughly determined by Qubit and later serially diluted while the final concentration was validated by Bio-Rad QX200 dPCR platform.

Table S1. Oligo DNA sequences

Oligo-DNAs	Sequence
prfA gene 280-bp fragment (template)	CCGCAAATAGAGCCAAGCTTCCCGTTAATCGAAAAATCATTAAATT TAGCTAGACTGTATGAAACTTGTTTTTGTAGGGTTTGGAAAACATA GAAAAAGTGCGTAAGATTCTTGCTCAGTAGTTCTTTTAGTTCGTTT ATTTTGATAACGTATGCGGTAGCCTGTTCGCTAATGACTTCTAAAT TATAATAGCCAACCGATGTTTCTGTATCAATAAAGCCAGACATTAT AACGAAAGCACCTTTGTAGTATTGTAAATTCATGATGGTCCCGTTC TCAC
Forward primer for template production	5’-CCGCAAATAGAGCCAAGCTT-3’
Reverse primer for template production	5’-GTGAGAACGGGACCATCATG-3’
Forward primer for TaqMan assay	5’-GCCTGTTCGCTAATGACTTCTAAAT-3’
Reverse primer for TaqMan assay	5’-GTGCTTTCGTTATAATGTCTGGCTTT-3’
TaqMan probe	FAM-5’-TAATAGCCAACCGATGTTT-3’-MGB

Table S2 lists the recipe of dPCR premix. The mixture was then loaded into MiCA tubes, and spun under 130,000 $m \cdot s^{-2}$ for 7 minutes leading to the liquid samples becoming 52.5 μm droplets with no dead volume. The emulsion droplets then went through two-step PCR thermocycling: 25 °C 10 min for surfactant encapsulation, 95 °C 2 min for enzyme activation, 40 cycles ramping (15 s at 94 °C and 30 s at 60 ° C) for amplification.

Table S2. Recipe of 2X premix for MiCA dPCR.

For 50 μl premix	Vol./ μl	Stock Conc.	Final Conc.
Polymerase Buffer †	10	10X	2X
$MgCl_2$ †	10	50 mM	10 mM

dNTP	4	10mM each	0.8 mM each
Forward Primer	5	20 μM	2 μM
Reverse Primer	5	20 μM	2 μM
TaqMan Probe	5	6 μM	600 nM
Platinum™ Taq Polymerase	1	10 U/μl	0.2 U/Rxn
Nuclease free water	10	--	--

† Both are from Platinum™ Taq polymerase kit

4. Digital counting of droplets

We modified the flow-chamber of a flow cytometer (BD FACS Jazz) to detect the droplets, both the fluorescent (Taqman probe positive) and non-fluorescent (Taqman probe negative) ones. Emulsion droplets were pumped into an inlet of a T-junction along with diluting oil into the other inlet (**Figure S2**). The diluted emulsion then flowed through a borosilicate glass micropipette with a tapering section in middle. A 488 nm laser was used for excitation. The fluorescence signals are collected by a PMT which voltage are measured by a high-speed DAQ card (National Instruments myDAQ).

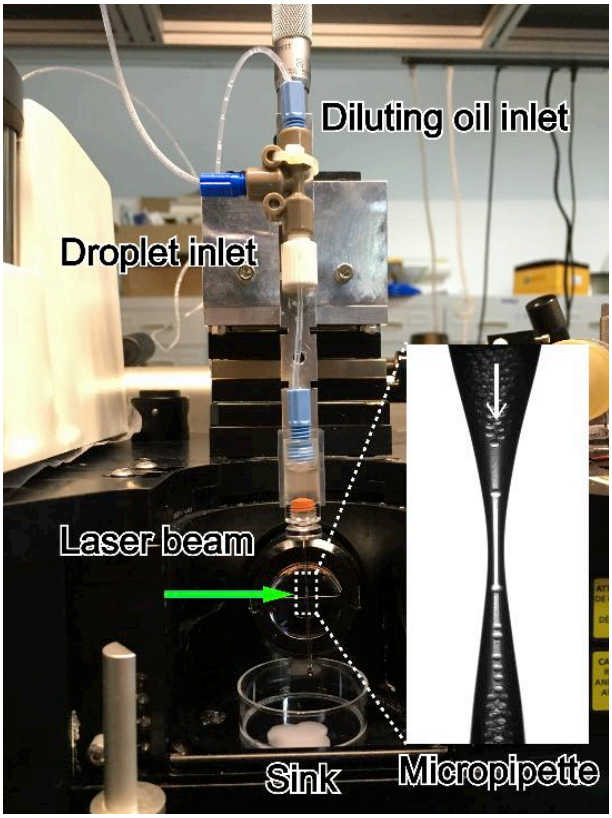

Figure S2. Modified flow chamber for droplet counting using a flow cytometer.

Taper fabrication: The borosilicate micropipettes (Sutter B100-30-7.5HP) were pulled using a capillary puller (Sutter P-1000). After 11 cycles of heat-pulling (Heat 500℃, Pull 2 times, Velocity 2, Time 5 s, Pre 500℃, Ramp 500℃), a tapered neck was formed with internal diameter ~100 μm.

5. Signal Analyze

We use MATLAB to analyze the signal captured by the DAQ card. Our program finds the pulses of the fluorescence signal. Each pulse indicates one droplet flowing through the detecting area, whose height is taken as the fluorescence intensity of the droplet. The distribution of fluorescence intensity of all the droplets in one experiment is shown in the Figure S3. As there were very few signals that fell between the two main peaks of the histogram, a threshold was set to 2 V to assign the 'positive' and the 'negative'.

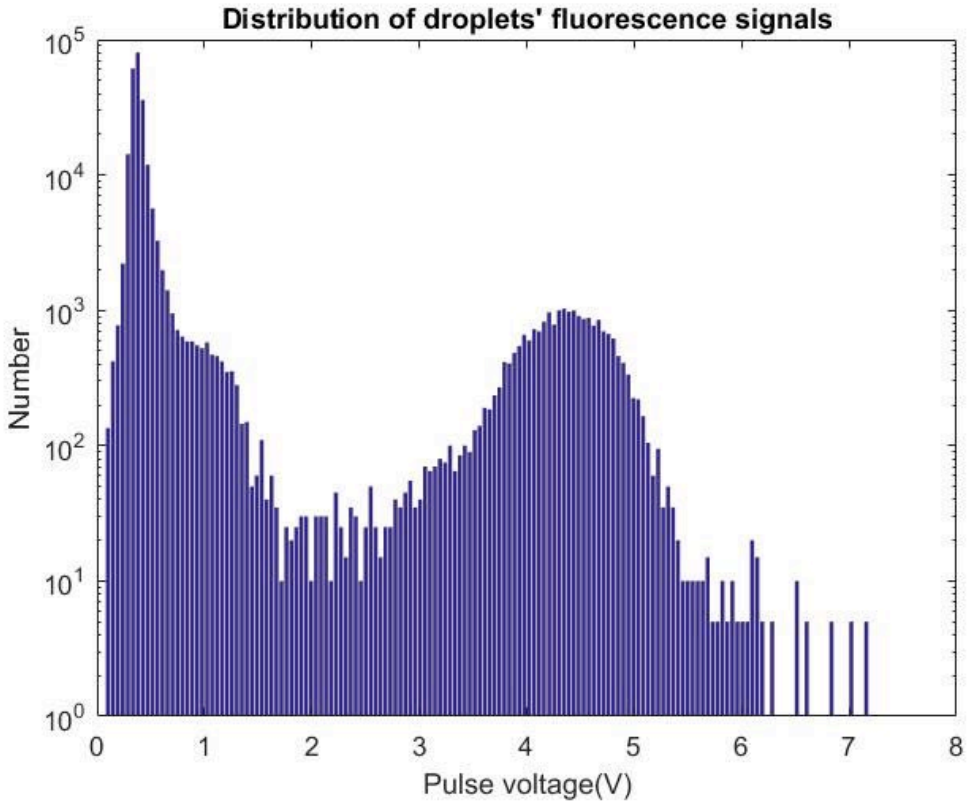

Figure S3. Pulse voltage distribution of dPCR droplets in a typical sample.

6. MiCA dPCR data analysis

Aqueous sample of volume *V* is divided into *N* partitions, average volume of each partition $\bar{v}$, and *m* copies of DNA template are dispensed in it. After Poisson process, *n* partitions/droplets signal positive. Define

$$p \stackrel{\text{def}}{=} \frac{n}{N} \qquad \text{Eq S1}$$

$$\lambda \stackrel{\text{def}}{=} \frac{m}{N} \qquad \text{Eq S2}$$

The purpose is to determine λ thus to get template concentration

$$C \triangleq^{\text{def}} \frac{m}{V} = \frac{\lambda N}{V}$$ Eq S3

Of a given droplet, the probability of having at least one template is

$$\rho = 1 - (1 - \frac{1}{N})^m$$ Eq S4

And when *N* is great enough,

$$\rho \approx 1 - e^{-\frac{m}{N}} = 1 - e^{-\lambda}$$ Eq S5

Thus for *N* droplet, the positive number *n* follows binomial distribution $n \sim \mathrm{B}(\rho, N)$, whose expectance and variance are

$$\mathrm{E}(n) = N(1 - e^{-\lambda})$$ Eq S6

$$\mathrm{D}(n) = Ne^{-\lambda}(1 - e^{-\lambda})$$ Eq S7

And for $p = \frac{n}{N}$,

$$\mathrm{E}(p) = 1 - e^{-\lambda}$$ Eq S8

$$\mathrm{D}(p) = e^{-\lambda}(1 - e^{-\lambda})/N$$ Eq S9

Therefore

$$\lambda = -\ln [1 - \mathrm{E}(p)]$$ Eq S10

We use p as an unbiased estimate for $\mathrm{E}(p)$, therefore it can be estimated that

$$\hat{\lambda} = -\ln (1 - p)$$ Eq S11

In the practice of MiCA dPCR, we examine *N*' droplets out of population *N*, and n' among *N*' droplets are found positive. The effective droplet rate *κ* can be expressed as follows.

$$\kappa = \frac{N\prime}{N}$$ Eq S12

Since in our experiment, effective droplet rate *κ* is above 80%, it is reasonable to assume

$$\frac{n}{N} = \frac{n\prime}{N\prime}$$ Eq S13

thus

$$\hat{\lambda} = -\ln (1 - \frac{n\prime}{N\prime})$$ Eq S14

In the practice of dPCR, *N* is also an estimate. To estimate *N*, one should either count all the droplet to have the exact value of *N*, or assume all the droplets are perfectly monodispersing, thus

$$N = \frac{V}{\bar{v}}$$ Eq S15

$$\hat{C} = -\ln (1 - \frac{n\prime}{N\prime}) \frac{1}{\bar{v}}$$ Eq S16

Where

$$\bar{v} = \frac{4\pi r^3}{3}$$ Eq S17